

Positional disorder in ammonia borane at ambient conditions

E. Welchman,¹ P. Giannozzi,² and T. Thonhauser^{1,*}

¹*Department of Physics, Wake Forest University, Winston-Salem, NC 27109, USA*

²*Department of Chemistry, Physics, and Environment, University of Udine, 33100 Udine, Italy*

(Dated: February 29, 2024)

We solve a long-standing experimental discrepancy of NH_3BH_3 , which—as a molecule—has a three-fold rotational axis, but in its crystallized form at room temperature shows a four-fold symmetry around the same axis, creating a geometric incompatibility. To explain this peculiar experimental result, we study the dynamics of this system with *ab initio* Car-Parrinello molecular dynamics and nudged-elastic band simulations. We find that rotations, rather than spatial static disorder, at angular velocities of 2 rev/ps—a time-scale too small to be resolved by standard experimental techniques—are responsible for the four-fold symmetry.

PACS numbers: 61.50.Ah, 65.40.-b, 88.30.R-, 63.20.dk

Ammonia borane NH_3BH_3 has drawn significant interest in recent years because of its potential as a hydrogen storage material, with a gravimetric storage density of 19.6 mass%.^{1–7} The structure of its solid phase has been explored previously,^{8–13} but the literature does not agree about the hydrogen behavior at room temperature. The molecule consists of a dative B–N bond and a trio of H atoms (henceforth referred to as a ‘halo’) bonded to each of those two atoms, forming an hourglass shape, visible in Fig. 1. At low temperatures (0 ~ 225 K), the solid exhibits an orthorhombic structure with space group $Pmn2_1$. Heated above 225 K, it undergoes a phase transition to a body-centered tetragonal structure with space group $I4mm$. It is this room-temperature phase that exhibits unexpected experimental results: while the molecule itself has a three-fold symmetry about the B–N axis, neutron^{11,14} and X-ray^{12,15,16} diffraction on the solid reveal a four-fold symmetry about the same axis, creating a geometric incompatibility within the structure. Investigating the dynamics of the system with *ab initio* methods, we find that the individual halos are rotating with angular velocity on the order of 0.7 deg/fs \approx 2 rev/ps, such that standard experiments can only probe the time averaged positions, leading to the tetragonal host structure with four-fold symmetry.

The precise behavior of these hydrogen halos has been the subject of several studies over three decades. In 1983, Reynhardt and Hoon⁸ found three-fold reorientations of the BH_3 and NH_3 groups with a tunneling frequency of 1.4 MHz in the orthorhombic phase. Penner et al.⁹ found in 1999 that these groups reoriented independently. Deciphering the behavior in the tetragonal structure has been less straightforward. In the same 1983 study, Reynhardt and Hoon concluded that the BH_3 , and possibly the NH_3 groups, rotate freely. Brown et al.¹¹ found that they could describe the disorder entirely with three-fold jump diffusion. Bowden et al. tried using a larger unit cell to model the same disorder as spatial variation rather than higher-order rotation; however, they found no evidence to support this model,¹² leaving this disagreement unre-

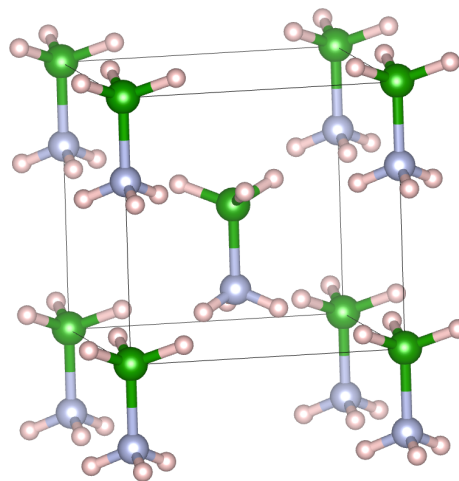


FIG. 1. Structure of the high-temperature, body-centered tetragonal phase of NH_3BH_3 . Note that the locations of H atoms in this figure are not indicative of experimental results, but just one possibility of how the halos could be oriented in the solid.

solved in the literature. The present study aims to elucidate how the hydrogen halos behave in the solid, especially in the high-temperature, tetragonal structure. To this end, we find thermal barriers to rotation in gas phase as well as both orthorhombic and tetragonal phases. We supplement these findings with *ab initio* molecular dynamics simulations to track individual halos’ behavior.

Our *ab initio* simulations are at the density functional theory level, using a plane-wave basis. Since ammonia borane is a strong van der Waals complex,^{16,17} the inclusion of van der Waals forces is essential,^{10,18,19} we thus use vdW-DF1^{20–22} (i.e. revPBE exchange and LDA correlation in addition to the nonlocal contribution) as the exchange-correlation functional for all calculations. Car-Parrinello molecular dynamics (CPMD) was performed with the CP code (part of QUANTUM-ESPRESSO version 5.0.2; the vdW-DF capability in CP is a new feature, which we have just implemented),²³ using ultrasoft

pseudopotentials and wave function and density cutoffs of 475 and 5700 eV. The CPMD simulations used an electronic convergence of 10^{-8} eV, a fictitious electron mass of 400 a.u., and a time step of 5 a.u. We further used a $2 \times 2 \times 2$ supercell, accommodating 16 molecules, and started from the experimental lattice constants¹² at 297 and 90 K for tetragonal and orthorhombic phases, respectively. Similar calculations have been done previously,²⁴ but with a different functional and at much higher temperature. Climbing image nudged-elastic band (NEB) simulations to find precise rotational barriers for halos and entire molecules were performed with VASP (version 5.3.3),^{25,26} utilizing PAW potentials and a cutoff of 500 eV. For solid phase barrier calculations, we used a $4 \times 4 \times 4$ k -point mesh and 8 images for NEB calculations. In the gas phase, we used only the gamma point and 16 images. Note that nuclear quantum effects have not been taken into account. Further information, in particular including structural information for all our simulations, can be found in the Supplementary Materials.

We begin by investigating the barriers for rotations in different situations, i.e. the gas-phase molecule and the orthorhombic and tetragonal solid phases. Depending on the situation, we performed two kinds of simulations: “fixed” labels simulations where the geometry of the cell as well as the halo has been fixed and the entire halo or molecule is rotated around the axis in a rigid manner. “NEB” refers to the transition state formalism of the nudged-elastic band method, where the geometry of the halo can change and adapt along the path, allowing it to lower its energy. While the latter is preferable due to its higher accuracy for barriers, we also use the former i) in order to compare to previous quantum-chemistry calculations; and ii) for the tetragonal high-temperature phase, in which NEB leads to unphysical deformations, as all DFT ground-state simulations are technically done at 0 K and the structure attempts to mimic the orthorhombic phase. Results are summarized in Table I and detailed curves for the barriers can be found in the Supplementary Materials.

The situation in the gas-phase molecule is the simplest. Completing a fixed rotation of one halo results in a thermal barrier of 84.7 meV, within 5% of an empirical estimate²⁷ and in very good agreement with quantum-chemistry calculations,²⁸ validating our methodology. NEB calculations necessarily decrease the estimate of the barrier, in this case yielding a value of 79.1 meV.

In a crystalline environment, dihydrogen bonds between molecules affect how each molecule behaves. In the orthorhombic phase, the dihydrogen bond network creates a 67.5 meV barrier to rotating the entire molecule (NEB). This barrier is low enough that molecules in a crystal can reorient at some rate, given enough temperature. It is interesting to see that a calculation with fixed halo geometry results in a much higher barrier, attesting to the fact that the rotating halo and its surroundings prefer to undergo significant deformation and reorientation during the rotation. For instance, the orientation of

TABLE I. Numerical values for calculated rotational barriers in meV and values given in the literature. Error bars for experimental values in the literature typically range from 5 to 10 meV.

	fixed	NEB	literature			
gas phase						
one halo	84.7	79.1	89.8, ^{a*} 86.7 ^{b‡}			
orthorhombic phase						
N halo	106.6	94.9	100, ^{c*} 142, ^{d*} 82.7, ^{e*} 131.6 ^{f†‡}			
B halo	443.9	102.9	260, ^{c*} 259, ^{d*} 397 ^{f†}			
molecule	403.4	67.5	328 ^{f†}			
tetragonal phase						
N halo	60.1		75.7, ^{d*} 50.8 ^{e*}			
B halo	61.9		60.8, ^{c*} 61.1, ^{d*} 50.8 ^{e*}			
molecule	19.4					

^aRef. 27, ^bRef. 28, ^cRef. 8, ^dRef. 9, ^eRef. 11, ^fRef. 29

[†]DFT (B3LYP), ^{††}quantum chemistry, *experiment

the B-N axis prefers to precess as the B halo is rotated in an attempt to maximize the strength of dihydrogen bonds with its neighbors.

The ease of the rotation process is dependent on which individual halo is rotated. Our calculations for the N halo barriers are in good agreement with experimental findings (summarized in Table I). Accuracy for the B halo is more difficult to gauge. Our results for a fixed rotation are in agreement with a previous theoretical study,²⁹ but experimental values line up almost exactly halfway between our calculations for fixed rotation and NEB barriers. Regardless of the magnitude of the difference, we find that the BH₃ group faces a larger barrier to rotation than the NH₃ group, in agreement with the literature.

In the high-temperature tetragonal phase, the rotation of either halo has essentially the same barrier of ~ 61 meV, in good agreement with the literature (again see Table I). But, even more important, rotating the entire molecule requires just 19.4 meV. This barrier is easily overcome at ambient conditions ($k_B T = 25$ meV at room temperature). Previous studies have argued that NH₃ and BH₃ groups rotate freely⁸ and that the molecule rotates as a whole.⁹ Our evidence supports a combination of both explanations. The barrier to rotating the whole molecule is low enough that it can occur freely at room temperature. The torsional barrier for each group also allows them to rotate independently; since these barriers are within 2 meV, this rate should be equivalent between the groups, leading atoms in both groups to move at the same rate, as seen experimentally.¹¹ Based on the barriers in Table I, from the Arrhenius equation we estimate (assuming the same pre-exponential factor for all rotations) that whole-molecule rotation occurs at about five times the rate of individual halo rotations at room temperature and approximately 20 and 30 times the rate for rotating individual halos in the low-temperature phase.

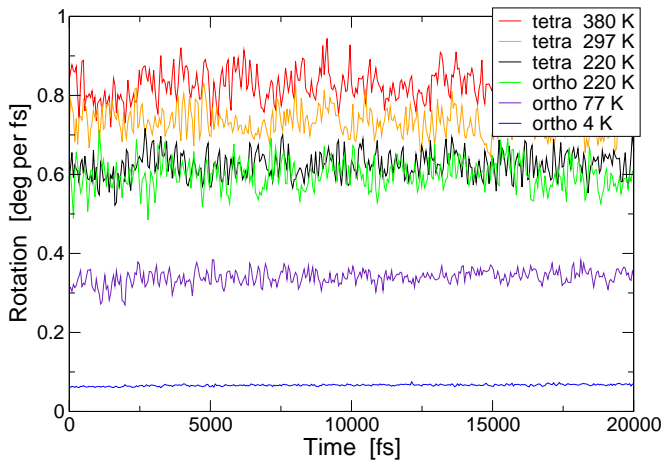


FIG. 2. Average angular velocity among H atoms at each frame in the simulation. The plot shows a running average over 50 frames. Note that this analysis only captures the angular velocity—motion of the single hydrogen atoms in a direction parallel to the B–N bond is not captured here, making up for some of the “missing” kinetic energy and keeping the temperature constant.

Also of note is that torsional barriers in the orthorhombic phase are larger than those of an isolated molecule, whereas the torsional barriers in the tetragonal phase are lower. This result alone shows that in the low-temperature phase rotation is suppressed, while it is encouraged in the high-temperature phase.

With the knowledge of the barriers, we now move to the analysis of the dynamics of the crystalline phase. We performed CPMD simulations in both the orthorhombic (at 4, 77, and 220 K) and tetragonal (at 220, 297, and 380 K) phases in order to study the motion of H atoms in the NH_3 and BH_3 groups. We used 1 ps for thermalization of the system and thereafter performed 20 ps production runs. Analyzing the corresponding trajectories leads to the initial (obvious) conclusion that halos rotate more rapidly at higher temperatures.

To substantiate this claim, we calculated for each H atom in the simulation the angular velocity about the nearest B–N axis. We then averaged the absolute value of this angular velocity—otherwise there is a lot of cancellation, as halos rotate in both directions—over all H atoms in the simulation to measure how rapidly the halos are rotating in each frame of the simulation. The results of this calculation are shown in Fig. 2, confirming the idea that H atoms rotate more quickly at higher temperatures and giving quantitative values for the speed of their rotation, in qualitative agreement with the barriers found earlier. It is important to note that in simulating the tetragonal supercell, the B–N axes typically maintain an instantaneous tilt between 5 and 20 degrees from vertical. At 297 and 380 K, the average orientation is vertical, whereas at 220 K there appears to be a correlation between neighbors similar to that found in the low-temperature phase. Consequently, the dynamics of

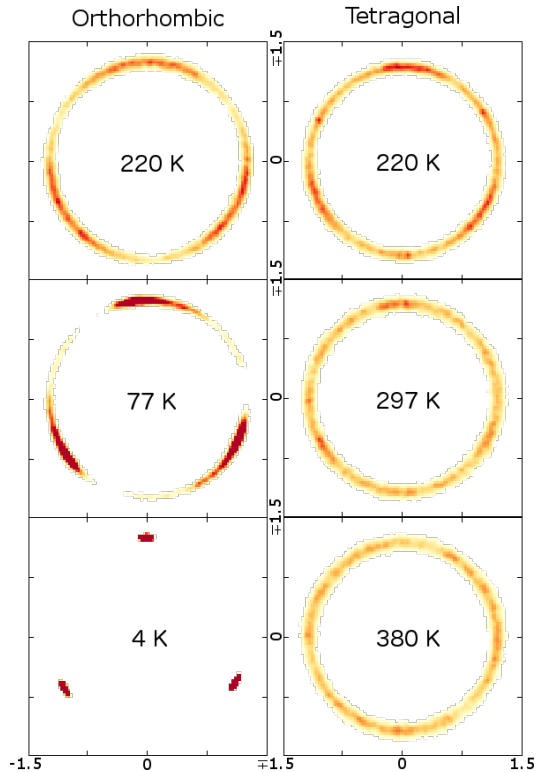


FIG. 3. Heat maps of the location of all three H atoms in one N-group halo over the course of CPMD simulations. The corresponding B-group heat maps look very similar. Positions have been flattened into a plane perpendicular to the B–N axis. Motion along this axis is not apparent in these plots. Each map is 3 \AA^2 .

the 220 K simulations are qualitatively very similar.

The order of magnitude for rotations is found to be $0.7 \text{ deg/fs} \approx 2 \text{ rev/ps}$ at room temperature. As such, halos can easily rotate 120 deg in 0.2 ps. Unless experiments can be performed with a resolution smaller than this, they will see time-averaged positions, and halos (with a three-fold symmetry) start looking like rings, as described below. Experiments will thus pick up the symmetry of the tetragonal host lattice, explaining the four-fold symmetry.

Casual observation of the simulations reveals that halos in the high-temperature phase are unlikely to undergo full revolutions in a short burst. Rather, a more accurate description of the qualitative behavior is that—as a halo moves close to a neighboring halo—they will rotate some amount in order to form a dihydrogen bond. The halo will then move closer to a different neighbor and adopt a different alignment. A halo equally far from all of its neighbors will also follow the realignment of the opposite halo of the same molecule. Because the molecules are constantly oscillating in the crystal structure due to thermal energy, these reorientation processes result in a constantly shifting dihydrogen bond network.

This analysis above describes how rapidly H atoms rotate about their native molecules, but does not describe

where they are. To give a more systematic estimate of hydrogen position over time, we provide “heat maps” in Fig. 3 that describe what angular positions the H atoms inhabit over the course of a whole simulation. Each heat map shows the occupation density for all three H atoms in a particular halo. These heat maps demonstrate a clear pattern of increasing positional disorder at higher temperature. The three-fold symmetry inherent in the molecular structure is apparent in the maps from the orthorhombic phase. This symmetry becomes much less clear in the tetragonal phase, indicating that rotation represents a significant source of the disorder found experimentally. Furthermore, the occupational density in the higher-temperature structure is much more spread out angularly, indicating that reorientation is not limited to 120-degree jumps, as concluded by Brown et al.,¹¹ but is a more fluid process.

In summary, we have calculated torsional and rotational barriers for NH_3BH_3 in the gas phase and both

low- and high-temperature crystalline structures. In addition, we have studied the dynamics of the crystalline phase explicitly with CPMD simulations. Our calculations indicate that in the low-temperature orthorhombic phase, the BH_3 and NH_3 groups reorient along a three-fold rotational potential at different rates. Both entire-molecule and independent reorientations contribute to the experimental rates found previously. In the high-temperature tetragonal phase, on the other hand, the barrier to entire-molecule rotation is low enough that thermal energy in ambient conditions allows the molecule to overcome the three-fold rotational potential. Consequently, the molecule is able to rotate freely with angular velocities on the order of 2 rev/ps. By quantifying the speed of those rotations, we thus resolve a long-standing experimental discrepancy, where a molecule with three-fold symmetry shows four-fold symmetry around the same axis in its crystalline form.

This work was supported in full by NSF Grant No. DMR-1145968.

* thonhauser@wfu.edu

- ¹ Z. Xiong, C. K. Yong, G. Wu, P. Chen, W. J. Shaw, A. Karkamkar, T. Autrey, M. O. Jones, S. R. Johnson, P. P. Edwards, and W. I. F. David, *Nat. Mater.* **7**, 138 (2008).
- ² Y. S. Chua, P. Chen, G. Wu, and Z. Xiong, *Chem. Commun.* **47**, 5116 (2011).
- ³ S. Swinnen, V. S. Nguyen, and M. T. Nguyen, *Chem. Phys. Lett.* **489**, 148 (2010).
- ⁴ C. W. Hamilton, R. T. Baker, A. Staubitz, and I. Manners, *Chem. Soc. Rev.* **38**, 279 (2009).
- ⁵ D. J. Heldebrant, A. Karkamkar, N. J. Hess, M. E. Bowden, S. Rassat, F. Zheng, K. Rappe, and T. Autrey, *Chem. Mater.* **20**, 5332 (2008).
- ⁶ T. B. Marder, *Angew. Chemie Int. Ed.* **46**, 8116 (2007).
- ⁷ H. Kim, A. Karkamkar, T. Autrey, P. Chupas, and T. Proffen, *J. Am. Chem. Soc.* **131**, 13749 (2009).
- ⁸ E. C. Reynhardt and C. F. Hoon, *J. Phys. C Solid State Phys.* **16**, 6137 (1983).
- ⁹ G. H. Penner, Y. C. P. Chang, and J. Hutzal, *Inorg. Chem.* **38**, 2868 (1999).
- ¹⁰ W. T. Klooster, T. F. Koetzle, P. E. M. Siegbahn, T. B. Richardson, and R. H. Crabtree, *J. Am. Chem. Soc.* **121**, 6337 (1999).
- ¹¹ C. M. Brown, T. L. Jacques, N. J. Hess, L. L. Daemen, E. Mamontov, J. C. Linehan, A. C. Stowe, and T. Autrey, *Phys. B Condens. Matter* **385–386**, 266 (2006).
- ¹² M. E. Bowden, G. J. Gainsford, and W. T. Robinson, *Aust. J. Chem.* **60**, 149 (2007).
- ¹³ Y. Lin, H. Ma, C. W. Matthews, B. Kolb, S. Sinogeikin, T. Thonhauser, and W. L. Mao, *J. Phys. Chem. C* **116**, 2172 (2012).
- ¹⁴ R. S. Kumar, X. Ke, J. Zhang, Z. Lin, S. C. Vogel, M. Hartl, S. Sinogeikin, L. Daemen, A. L. Cornelius, C. Chen, and Y. Zhao, *Chem. Phys. Lett.* **495**, 203 (2010).
- ¹⁵ Y. Filinchuk, A. Nevidomskyy, D. Chernyshov, and V. Dmitriev, *Phys. Rev. B* **79**, 214111 (2009).
- ¹⁶ J. Chen, H. Couvy, H. Liu, V. Drozd, L. L. Daemen, Y. Zhao, and C.-C. Kao, *Int. J. Hydrogen Energy* **35**, 11064 (2010).
- ¹⁷ Y. Lin, W. L. Mao, V. Drozd, J. Chen, and L. L. Daemen, *J. Chem. Phys.* **129**, 234509 (2008).
- ¹⁸ D. J. Wolstenholme, J. T. Titah, F. N. Che, K. T. Trauboulee, J. Flogeras, and G. S. McGrady, *J. Am. Chem. Soc.* **133**, 16598 (2011).
- ¹⁹ D. J. Wolstenholme, K. T. Trauboulee, Y. Hua, L. A. Calhoun, and G. S. McGrady, *Chem. Commun.* **48**, 2597 (2012).
- ²⁰ M. Dion, H. Rydberg, E. Schröder, D. C. Langreth, and B. I. Lundqvist, *Phys. Rev. Lett.* **92**, 246401 (2004).
- ²¹ T. Thonhauser, V. R. Cooper, S. Li, A. Puzder, P. Hyldgaard, and D. C. Langreth, *Phys. Rev. B* **76**, 125112 (2007).
- ²² D. C. Langreth, B. I. Lundqvist, S. D. Chakarova-Käck, V. R. Cooper, M. Dion, P. Hyldgaard, A. Kelkkanen, J. Kleis, L. Kong, S. Li, P. G. Moses, E. D. Murray, A. Puzder, H. Rydberg, E. Schröder, and T. Thonhauser, *J. Phys. Condens. Matter* **21**, 084203 (2009).
- ²³ P. Giannozzi, S. Baroni, N. Bonini, M. Calandra, R. Car, C. Cavazzoni, D. Ceresoli, G. L. Chiarotti, M. Cococcioni, I. Dabo, A. Dal Corso, S. de Gironcoli, S. Fabris, G. Fratesi, R. Gebauer, U. Gerstmann, C. Gougousis, A. Kokalj, M. Lazzeri, L. Martin-Samos, N. Marzari, F. Mauri, R. Mazzarello, S. Paolini, A. Pasquarello, L. Paulatto, C. Sbraccia, S. Scandolo, G. Sclauszero, A. P. Seitsonen, A. Smogunov, P. Umari, and R. M. Wentzcovitch, *J. Phys. Condens. Matter* **21**, 395502 (2009).
- ²⁴ Y. Liang and J. S. Tse, *J. Phys. Chem. C* **116**, 2146 (2012).
- ²⁵ G. Kresse and J. Furthmüller, *Phys. Rev. B* **54**, 11169 (1996).
- ²⁶ G. Kresse and D. Joubert, *Phys. Rev. B* **59**, 1758 (1999).
- ²⁷ L. R. Thorne, R. D. Suenram, and F. J. Lovas, *J. Chem. Phys.* **78**, 167 (1983).
- ²⁸ J. Demaison, J. Liévin, A. G. Császár, and C. Gutle, J.

- Phys. Chem. A **112**, 4477 (2008).
- ²⁹ V. M. Parvanov, G. K. Schenter, N. J. Hess, L. L. Daemen, M. Hartle, A. C. Stowe, D. M. Camaioni, and T. Autrey, Dalton Trans. **33**, 4514 (2008).

Positional disorder in ammonia borane at ambient conditions — Supplemental Material —

E. Welchman,¹ P. Giannozzi,² and T. Thonhauser^{1,*}

¹*Department of Physics, Wake Forest University, Winston-Salem, NC 27109, USA*

²*Department of Chemistry, Physics, and Environment, University of Udine, 33100 Udine, Italy*

(Dated: February 29, 2024)

I. OPTIMIZED STRUCTURES

A. Isolated Molecule

Cartesian coordinates (x , y , z) in Å, for the optimized structure found by our simulations of an isolated NH_3BH_3 molecule.

B	0.0000000	0.0000000	0.0000000
N	0.0000000	1.6856212	0.0000000
H	0.9519811	2.0563251	0.0000000
H	-1.1740483	-0.3022489	0.0000000
H	-0.4759065	2.0567762	0.8242625
H	-0.4759065	2.0567762	-0.8242625
H	0.5870187	-0.3021106	-1.0167601
H	0.5870187	-0.3021106	1.0167602

B. Orthorhombic Structure

Lattice parameters and fractional coordinates (x/a , y/b , and z/c) resulting from our simulations optimizing the structure of NH_3BH_3 in the low-temperature, orthorhombic phase.

$$\begin{aligned} a &= 5.44233 \text{ Å} \\ b &= 4.94048 \text{ Å} \\ c &= 5.13446 \text{ Å} \\ \alpha &= \beta = \gamma = 90.0^\circ \end{aligned}$$

B	0.0000000	0.1830125	0.0019077
B	0.5000000	0.8169874	0.5019076
N	0.0000000	0.2402808	0.3127204
N	0.5000000	0.7597191	0.8127204
H	0.0000000	0.4427503	0.3555205
H	0.5000000	0.5572496	0.8555205
H	0.1520232	0.1583956	0.4010154
H	0.3479767	0.8416043	0.9010154
H	0.6520232	0.8416043	0.9010154
H	0.8479767	0.1583956	0.4010154
H	0.0000000	0.9368787	0.9737231
H	0.5000000	0.0631212	0.4737231
H	0.1851884	0.2836140	0.9105986
H	0.3148115	0.7163859	0.4105986
H	0.6851884	0.7163859	0.4105986
H	0.8148115	0.2836140	0.9105986

C. Tetragonal Structure — From Experiment

Lattice parameters and fractional coordinates (x/a , y/b , and z/c) of the high-temperature, tetragonal structure of NH_3BH_3 , taken from experiment and refined in space group $I4mm$. Taken directly from Ref. 1.

$$\begin{aligned} a &= b = 5.2630 \text{ Å} \\ c &= 5.0504 \text{ Å} \end{aligned}$$

B	0.0000	0.0000	0.0032
N	0.0000	0.0000	0.6869
H	0.0000	0.1480	0.6190
H	0.0000	0.1990	0.0770

D. Tetragonal Structure — For Calculations

Lattice parameters and fractional coordinates (x/a , y/b , and z/c) used for the high-temperature, tetragonal structure of NH_3BH_3 . The structure from Ref. 1 was used as a starting point. Hydrogen halos were completed to include twelve atoms in order to demonstrate both four-fold and three-fold rotational symmetries. We then found the energy of each possible arrangement of the three-atom halos out of these available positions where each molecule retained its characteristic three-fold symmetry. The arrangement with the lowest energy is shown here:

$$\begin{aligned} a &= b = 5.2630 \text{ Å} \\ c &= 5.0504 \text{ Å} \end{aligned}$$

B	0.0000000	0.0000000	0.0032000
B	0.5000000	0.5000000	0.5032000
N	0.0000000	0.0000000	0.6869000
N	0.5000000	0.5000000	0.1869000
H	0.8010000	0.0000000	0.0770000
H	0.0995000	0.1723390	0.0770000
H	0.0995000	0.8276610	0.0770000
H	0.1480000	0.0000000	0.6190000
H	0.9260000	0.8718280	0.6190000
H	0.9260000	0.1281720	0.6190000
H	0.4005000	0.6723390	0.5770000
H	0.6990000	0.5000000	0.5770000
H	0.4005000	0.3276610	0.5770000
H	0.5740000	0.3718282	0.1190000
H	0.3519998	0.5000000	0.1190000
H	0.5740002	0.6281719	0.1190000

II. MOLECULAR DYNAMICS SIMULATIONS

For our molecular dynamics calculations, we used the CP code (part of QUANTUM-ESPRESSO), utilizing ultra-soft pseudopotentials and wave function and density cutoffs of 475 and 5700 eV with an electronic convergence of 10^{-8} eV, a fictitious electron mass of 400 a.u., and a time step of 5 a.u. We used a Nosé thermostat with an oscillation frequency of 6.5 THz and allowed the simulations to thermalize for at least 1 ps. Production runs were typically at least 20 ps. The starting structures are listed below.

A. Orthorhombic Structure

Starting fractional coordinates (x/a , y/b , and z/c) and lattice parameters used for CPMD calculations in the low-temperature, orthorhombic phase. A $2 \times 2 \times 2$ super-cell was used, including 16 NH_3BH_3 molecules.

$$\begin{aligned} a &= 10.88466 \text{ \AA} \\ b &= 9.88096 \text{ \AA} \\ c &= 10.26892 \text{ \AA} \\ \alpha &= \beta = \gamma = 90.0^\circ \end{aligned}$$

B	0.0000000	0.0804724	0.0009784
B	0.0000000	0.0804724	0.4901925
B	0.0000000	0.5566408	0.0009784
B	0.0000000	0.5566408	0.4901925
B	0.5090651	0.0804724	0.0009784
B	0.5090651	0.0804724	0.4901925
B	0.5090651	0.5566408	0.0009784
B	0.5090651	0.5566408	0.4901925
B	0.2545325	0.3956959	0.2455854
B	0.2545325	0.3956959	0.7347996
B	0.2545325	0.8718642	0.2455854
B	0.2545325	0.8718642	0.7347996
B	0.7635976	0.3956959	0.2455854
B	0.7635976	0.3956959	0.7347996
B	0.7635976	0.8718642	0.2455854
B	0.7635976	0.8718642	0.7347996
N	0.0000000	0.1170898	0.1526837
N	0.0000000	0.1170898	0.6418978
N	0.0000000	0.5932580	0.1526837
N	0.0000000	0.5932580	0.6418978
N	0.5090651	0.1170898	0.1526837
N	0.5090651	0.1170898	0.6418978
N	0.5090651	0.5932580	0.1526837
N	0.5090651	0.5932580	0.6418978
N	0.2545325	0.3590785	0.3972908
N	0.2545325	0.3590785	0.8865048
N	0.2545325	0.8352468	0.3972908
N	0.2545325	0.8352468	0.8865048
N	0.7635976	0.3590785	0.3972908
N	0.7635976	0.3590785	0.8865048
N	0.7635976	0.8352468	0.3972908
N	0.7635976	0.8352468	0.8865048
H	0.0000000	0.1971337	0.1629083
H	0.0000000	0.1971337	0.6521223
H	0.0000000	0.6733020	0.1629083
H	0.0000000	0.6733020	0.6521223
H	0.5090651	0.1971337	0.1629083
H	0.5090651	0.1971337	0.6521223
H	0.5090651	0.6733020	0.1629083
H	0.5090651	0.6733020	0.6521223
H	0.2545325	0.2790346	0.4075153
H	0.2545325	0.2790346	0.8967295
H	0.2545325	0.7552029	0.4075153
H	0.2545325	0.7552029	0.8967295
H	0.7635976	0.2790346	0.4075153

H	0.7635976	0.2790346	0.8967295
H	0.7635976	0.7552029	0.4075153
H	0.7635976	0.7552029	0.8967295
H	0.0717782	0.0795201	0.1932396
H	0.0717782	0.0795201	0.6824537
H	0.0717782	0.5556884	0.1932396
H	0.0717782	0.5556884	0.6824537
H	0.5808432	0.0795201	0.1932396
H	0.5808432	0.0795201	0.6824537
H	0.5808432	0.5556884	0.1932396
H	0.5808432	0.5556884	0.6824537
H	0.1827544	0.3966482	0.4378466
H	0.1827544	0.3966482	0.9270607
H	0.1827544	0.8728165	0.4378466
H	0.1827544	0.8728165	0.9270607
H	0.6918194	0.3966482	0.4378466
H	0.6918194	0.3966482	0.9270607
H	0.6918194	0.8728165	0.4378466
H	0.6918194	0.8728165	0.9270607
H	0.3263107	0.3966482	0.4378466
H	0.3263107	0.3966482	0.9270607
H	0.3263107	0.8728165	0.4378466
H	0.3263107	0.8728165	0.9270607
H	0.8353757	0.3966482	0.4378466
H	0.8353757	0.3966482	0.9270607
H	0.8353757	0.8728165	0.4378466
H	0.8353757	0.8728165	0.9270607
H	0.4372869	0.0795201	0.1932396
H	0.4372869	0.0795201	0.6824537
H	0.4372869	0.5556884	0.1932396
H	0.4372869	0.5556884	0.6824537
H	0.9463518	0.0795201	0.1932396
H	0.9463518	0.0795201	0.6824537
H	0.9463518	0.5556884	0.1932396
H	0.9463518	0.5556884	0.6824537
H	0.0000000	0.4428365	0.4862788
H	0.0000000	0.4428365	0.9754928
H	0.0000000	0.9190048	0.4862788
H	0.0000000	0.9190048	0.9754928
H	0.5090651	0.4428365	0.4862788
H	0.5090651	0.4428365	0.9754928
H	0.5090651	0.9190048	0.4862788
H	0.5090651	0.9190048	0.9754928
H	0.2545325	0.0333318	0.2416718
H	0.2545325	0.0333318	0.7308858
H	0.2545325	0.5095001	0.2416718
H	0.2545325	0.5095001	0.7308858
H	0.7635976	0.0333318	0.2416718
H	0.7635976	0.0333318	0.7308858
H	0.7635976	0.5095001	0.2416718
H	0.7635976	0.5095001	0.7308858
H	0.0789051	0.1309463	0.4490985
H	0.0789051	0.1309463	0.9383126
H	0.0789051	0.6071146	0.4490985
H	0.0789051	0.6071146	0.9383126
H	0.5879701	0.1309463	0.4490985
H	0.5879701	0.1309463	0.9383126
H	0.5879701	0.6071146	0.4490985
H	0.5879701	0.6071146	0.9383126
H	0.1756274	0.3452220	0.2044915
H	0.1756274	0.3452220	0.6937056
H	0.1756274	0.8213903	0.2044915
H	0.1756274	0.8213903	0.6937056
H	0.6846925	0.3452220	0.2044915
H	0.6846925	0.3452220	0.6937056
H	0.6846925	0.8213903	0.2044915
H	0.6846925	0.8213903	0.6937056
H	0.3334376	0.3452220	0.2044915
H	0.3334376	0.3452220	0.6937056
H	0.3334376	0.8213903	0.2044915
H	0.3334376	0.8213903	0.6937056
H	0.8425027	0.3452220	0.2044915
H	0.8425027	0.3452220	0.6937056
H	0.8425027	0.8213903	0.2044915
H	0.8425027	0.8213903	0.6937056
H	0.4301600	0.1309463	0.4490985
H	0.4301600	0.1309463	0.9383126
H	0.4301600	0.6071146	0.4490985
H	0.4301600	0.6071146	0.9383126
H	0.9392250	0.1309463	0.4490985
H	0.9392250	0.1309463	0.9383126
H	0.9392250	0.6071146	0.4490985
H	0.9392250	0.6071146	0.9383126

B. Tetragonal Structure

Starting fractional coordinates (x/a , y/b , and z/c) and lattice parameters used for CPMD calculations in the high-temperature, tetragonal phase.

$$a = b = 10.526 \text{ \AA}$$

$$c = 10.1008 \text{ \AA}$$

B	0.0000000	0.0000000	0.0016201
B	0.0000000	0.0000000	0.5016280
B	0.0000000	0.5000038	0.0016201
B	0.0000000	0.5000038	0.5016280
B	0.5000038	0.0000000	0.0016201
B	0.5000038	0.0000000	0.5016280
B	0.5000038	0.5000038	0.0016201
B	0.5000038	0.5000038	0.5016280
B	0.2500019	0.2500019	0.2516239
B	0.2500019	0.2500019	0.7516319
B	0.2500019	0.7500057	0.2516239
B	0.2500019	0.7500057	0.7516319
B	0.7500057	0.2500019	0.2516239
B	0.7500057	0.2500019	0.7516319
B	0.7500057	0.7500057	0.2516239
B	0.7500057	0.7500057	0.7516319
N	0.0000000	0.0000000	0.3434755
N	0.0000000	0.0000000	0.8434833
N	0.0000000	0.5000038	0.3434755
N	0.0000000	0.5000038	0.8434833
N	0.5000038	0.0000000	0.3434755
N	0.5000038	0.0000000	0.8434833
N	0.5000038	0.5000038	0.3434755
N	0.5000038	0.5000038	0.8434833
N	0.2500019	0.2500019	0.0934715
N	0.2500019	0.2500019	0.5934794
N	0.2500019	0.7500057	0.0934715
N	0.2500019	0.7500057	0.5934794
N	0.7500057	0.2500019	0.0934715
N	0.7500057	0.2500019	0.5934794
N	0.7500057	0.7500057	0.0934715
N	0.7500057	0.7500057	0.5934794
H	0.0000000	0.4259533	0.3095699
H	0.0000000	0.4259533	0.8095778
H	0.0000000	0.9259571	0.3095699
H	0.0000000	0.9259571	0.8095778
H	0.5000038	0.4259533	0.3095699
H	0.5000038	0.4259533	0.8095778
H	0.5000038	0.9259571	0.3095699
H	0.5000038	0.9259571	0.8095778
H	0.2500019	0.3240524	0.0595660
H	0.2500019	0.3240524	0.5595738
H	0.2500019	0.8240562	0.0595660
H	0.2500019	0.8240562	0.5595738
H	0.7500057	0.3240524	0.0595660
H	0.7500057	0.3240524	0.5595738
H	0.7500057	0.8240562	0.0595660
H	0.7500057	0.8240562	0.5595738
H	0.0000000	0.0999007	0.0389506
H	0.0000000	0.0999007	0.5389586
H	0.0000000	0.5999046	0.0389506
H	0.0000000	0.5999046	0.5389586
H	0.5000038	0.0999007	0.0389506
H	0.5000038	0.0999007	0.5389586
H	0.5000038	0.5999046	0.0389506
H	0.5000038	0.5999046	0.5389586
H	0.2500019	0.1501012	0.2889545
H	0.2500019	0.1501012	0.7889625
H	0.2500019	0.6501050	0.2889545
H	0.2500019	0.6501050	0.7889625
H	0.7500057	0.1501012	0.2889545
H	0.7500057	0.1501012	0.7889625
H	0.7500057	0.6501050	0.2889545
H	0.7500057	0.6501050	0.7889625
H	0.4316033	0.0395003	0.3095049
H	0.4316033	0.0395003	0.8095127
H	0.4316033	0.5395041	0.3095049
H	0.4316033	0.5395041	0.8095127
H	0.9316071	0.0395003	0.3095049
H	0.9316071	0.0395003	0.8095127

H	0.9316071	0.5395041	0.3095049
H	0.9316071	0.5395041	0.8095127
H	0.0684005	0.0395003	0.3095049
H	0.0684005	0.0395003	0.8095127
H	0.0684005	0.5395041	0.3095049
H	0.0684005	0.5395041	0.8095127
H	0.5684043	0.0395003	0.3095049
H	0.5684043	0.0395003	0.8095127
H	0.5684043	0.5395041	0.3095049
H	0.5684043	0.5395041	0.8095127
H	0.3184024	0.2105016	0.0595009
H	0.3184024	0.2105016	0.5595089
H	0.3184024	0.7105054	0.0595009
H	0.3184024	0.7105054	0.5595089
H	0.8184062	0.2105016	0.0595009
H	0.8184062	0.2105016	0.5595089
H	0.8184062	0.7105054	0.0595009
H	0.8184062	0.7105054	0.5595089
H	0.1816014	0.2105016	0.0595009
H	0.1816014	0.2105016	0.5595089
H	0.1816014	0.7105054	0.0595009
H	0.1816014	0.7105054	0.5595089
H	0.6816052	0.2105016	0.0595009
H	0.6816052	0.2105016	0.5595089
H	0.6816052	0.7105054	0.0595009
H	0.6816052	0.7105054	0.5595089
H	0.0866007	0.4505034	0.0385006
H	0.0866007	0.4505034	0.5385085
H	0.0866007	0.9505072	0.0385006
H	0.0866007	0.9505072	0.5385085
H	0.5866045	0.4505034	0.0385006
H	0.5866045	0.4505034	0.5385085
H	0.5866045	0.9505072	0.0385006
H	0.5866045	0.9505072	0.5385085
H	0.4134031	0.4505034	0.0385006
H	0.4134031	0.4505034	0.5385085
H	0.4134031	0.9505072	0.0385006
H	0.4134031	0.9505072	0.5385085
H	0.9134070	0.4505034	0.0385006
H	0.9134070	0.4505034	0.5385085
H	0.9134070	0.9505072	0.0385006
H	0.9134070	0.9505072	0.5385085
H	0.1634012	0.2995023	0.2885046
H	0.1634012	0.2995023	0.7885125
H	0.1634012	0.7995061	0.2885046
H	0.1634012	0.7995061	0.7885125
H	0.6634051	0.2995023	0.2885046
H	0.6634051	0.2995023	0.7885125
H	0.6634051	0.7995061	0.2885046
H	0.6634051	0.7995061	0.7885125
H	0.3366026	0.2995023	0.2885046
H	0.3366026	0.2995023	0.7885125
H	0.3366026	0.7995061	0.2885046
H	0.3366026	0.7995061	0.7885125
H	0.8366064	0.2995023	0.2885046
H	0.8366064	0.2995023	0.7885125
H	0.8366064	0.7995061	0.2885046
H	0.8366064	0.7995061	0.7885125

III. DETAILED ROTATIONAL BARRIERS

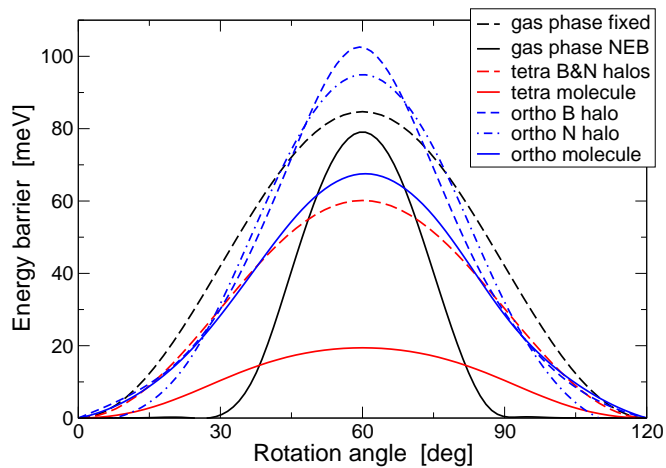


FIG. 1. Comparison of rotational barriers as obtained by NEB calculations and fixed-geometry calculations. The maxima of these curves are tabulated in Table 1 of the main manuscript.

* thonhauser@wfu.edu

¹ M. E. Bowden, G. J. Gainsford, and W. T. Robinson, Aust. J. Chem. **60**, 149 (2007).